

Original Research Paper

Computer Aid Screening for Potential Antimalarial Chloroquinone Compounds as Covid 19 Utilizing Computational Calculations and Molecular Docking Study

¹Asmaa Aboelnaga, ²Asmaa M. Fahim and ^{1,3}Taghreed H. EL-Sayed

¹Department of Chemistry, Faculty of Women of Arts, Science and Education, Ain Shams University, Heliopolis, Egypt

²Departments of Green Chemistry, National Research Center, Dokki, P.O. Box.12622 Cairo, Egypt

³Departments of Chemistry, Faculty of Science, Taibah University, Yanbu, Saudi Arabia

Article history

Received: 28-09-2020

Revised: 25-11-2020

Accepted: 30-11-2020

Corresponding Author:

Asmaa Aboelnaga
Department of Chemistry,
Faculty of Women of Arts,
Science and Education, Ain
Shams University, Heliopolis,
Egypt
Email:
asmaa.aboelnaga@women.as
u.edu.eg

And

Asmaa M Fahim
Departments of Green
Chemistry, National Research
Center, Dokki, P.O. Box.12622
Cairo, Egypt
Email:
asmaamahmoud8521@hotmail.
com

Abstract: Click reaction of 4,7-dichloroquinoline (1) with thiosemicarbazide (2) to afford the corresponding 2-(7-chloroquinolin-4-yl)thiosemicarbazide (3) utilized ultrasonic irradiation which can cyclized easily with ethylacetoacetate to give the 3-(7-chloroquinolin-4-ylamino)-tetrahydro-6-methyl-2-thioxopyrimidin-4(1*H*)-one (4) via nucleophilic substitution reaction. The synthesized compounds was examined *in vitro* antimalarial activity with $IC_{50} = 11.92, 25.37 \mu\text{g/mL}$ against chloroquinone drug. Furthermore, the theoretical investigation of most active compounds CQT and CQP utilizing of DFT/B3LYP/6-311G(d) and HF/6-311G(d) basis's set and evaluated their physical characters, bond length, bond angles, dihedral angles, also its HOMO-LUMO energy gap was 3.77 eV which indicate the reactivity of CQP. Moreover, the molecular docking studies of these synthesized compounds showed small energy affinity against SARS-CoV-2 main protease (PDBID: 6lu7) and crystal structure of thermoplasma acidophilum (PDBID: 1q2w) and shorter bond length. All these parameters could be considered with different extent to significantly affect the binding affinity of these compounds to the active protein sites for further biological evaluation on Covid-19.

Keywords: Covid 19, Novel Chloroquinone Compounds, Antimalarial Activity, Computational Studies, Docking Interaction

Introduction

In December 2019, several cases of pneumonia of an unknown etiology appeared in Wuhan, Hubei Province, China. Later, a novel coronavirus was identified in a bronchoalveolar lavage fluid sample from the Wuhan Seafood Market through the use of metagenomic next-generation sequencing technology (Yang and Wang, 2020; Wu *et al.*, 2020a). On February 11, 2020, the International Committee on Taxonomy of Viruses (ICTV) named the virus Severe Acute Respiratory Syndrome Coronavirus-2 (SARS-CoV-2). This is the seventh member of the coronavirus family that can infect humans after the appearance of Severe Acute Respiratory Syndrome Coronavirus (SARS-CoV) and

Middle East Respiratory Syndrome Coronavirus (MERS-CoV). The World Health Organization classified the coronavirus pneumonia epidemic caused by SARS-CoV-2 as a public health emergency of international concern on January 30, 2020 (Zhao *et al.*, 2010; Zhou *et al.*, 2020). A thorough program, including surveillance, diagnostics, clinical treatment, research and the development of vaccines and drugs, is crucial to win the battle against COVID-19 and other infectious diseases (Yang and Wang, 2020). Etiology of SARS-COV-2 Corona viruses are not new infectious pathogens in the world. The first described coronavirus was isolated from chickens in 1937 (Ludwig and Zarbock, 2020). In the mid-1960s the first human coronaviruses were first identified (Steardo *et al.*, 2020). The Corona virus family

can be divided into four genera: α , β , γ and δ , as per the genome structure and phylogenetic analysis of coronaviruses (Fehr and Perlman, 2015). The coronaviruses of the α and β mainly infect mammals and humans, while the coronaviruses of the γ and δ typically infect birds (Rodriguez-Morales *et al.*, 2020; Guo *et al.*, 2020). The pathogen that is causing the pandemic is related to the Acute Respiratory Syndrome Coronavirus (SARS-CoV), which caused another back outbreak in 2003 (Sjödén *et al.*, 2020; Mirza and Froeyen, 2020). As of yet, there are no effective treatments or targeted therapeutics against the virus. Because of that, the scientific community is striving to investigate many different mechanisms to interfere with the virus' metabolism. Consequently, in recent clinical trials against COVID-19 several antiviral drugs used with patients with similar viral infections to antimalarial drugs, such chloroquine (I), quinine (II) and amodiaquine (III) in malaria treatment is common (dos Santos Chagas *et al.*, 2019; Kwofie *et al.*, 2020). Also the hydroxychloroquine (IV) has approved drug for malaria disease treatment via the FDA was explored as a medication for SARS-CoV-2. As displayed in Figure 1 (Yao *et al.*, 2020; Liu *et al.*, 2020). Previous reports have shown that, the chloroquine and hydroxychloroquine can inhibit the Coronavirus (COVID-19) by altering the pH at the surface of the cell membrane. This can inhibit the attachment of the virus to the cell membrane. Furthermore, it can prevent nucleic acid replication, glycosylation of viral proteins, virus assembly, new virus particle delivery, virus release and other mechanisms to obtain its antiviral effects (Grimstein *et al.*, 2019).

The theoretical DFT calculations and the conformational analyses can result in a great contribution to drug discovery by reducing financial costs and saving time (especially for emerging diseases such as COVID-19 and speeding up analyses of target interactions with drug candidates (Gimeno *et al.*, 2019). As a result, different computational studies have been published to help better understand the mechanism of M-pro and try to inhibit its function (Mirza and Froeyen, 2020; Ton *et al.*, 2020; Kong *et al.*, 2020; Tang *et al.*, 2020; Chen *et al.*, 2020; Liu and Wang, 2020; Adem *et al.*, 2020; Yoshino *et al.*, 2020; Hosseini and Amanlou, 2020; Bzówka *et al.*, 2020a; 2020b; Khaerunnisa *et al.*, 2020; Xu *et al.*, 2020).

In this investigation, we concern in our work of theoretical determination of the molecular geometry of synthesized materials 2-(7-chloroquinolin-4-yl)thiosemicarbazide (3) (CQT) and 3-(7-chloroquinolin-4-ylamino)-tetrahydro-6-methyl-2-thioxopyrimidin-4(1H)-one (Aboelnaga and EL-Sayed, 2018) (4) (CQP) which exhibited excellent antimalarial activity against chloroquinone drug. Our stimulation was focused on confirmation of our compounds and comparison with 4,7-dichloroquinoline from physical properties, bond length, bond angles utilizing DFT/B3LYP/6-311G(d) and HF/6-311G(d) basis set (Hagar *et al.*, 2020; Arif *et al.*, 2020; Wu *et al.*, 2020b). Furthermore, the molecular docking studies of these compounds against target main protease (Mpro) of SARS-CoV-2: Mpro (PDBID: 6lu7) and crystal structure of thermoplasma acidophilum (PDBID: 1qw2) to know the binding interaction energy and interaction hydrogen bonding between our compounds and the different protein's sites.

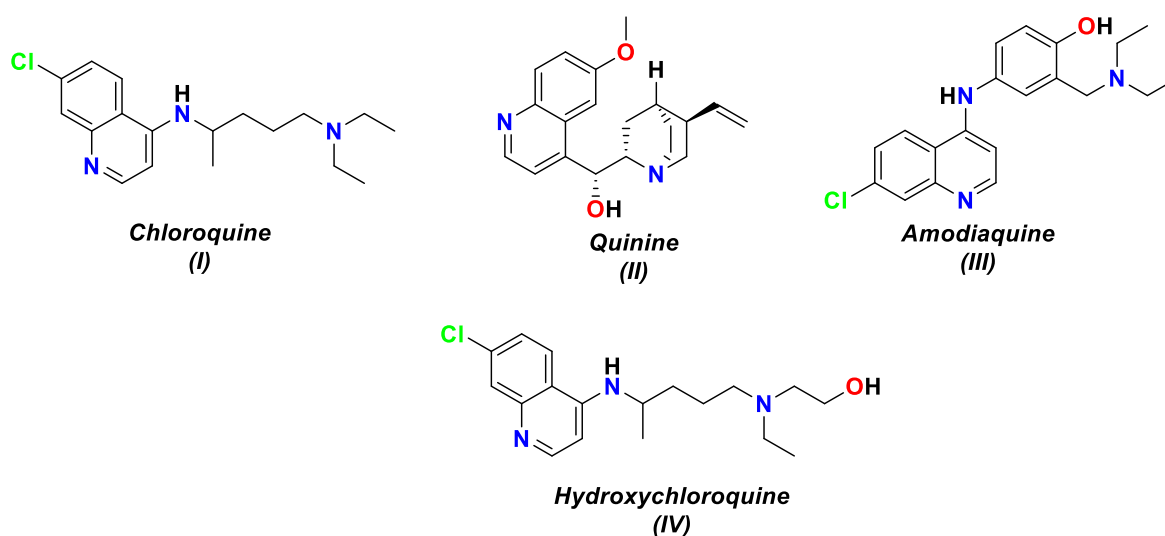


Fig. 1: Some of antimalarial drugs attached to quinolone ring

Results and Discussion

Chemistry

The nucleophilic substitution reaction 4,7-dichloroquinoline (1) with thiosemicarbazide (2) utilizing ultrasonic irradiation for 30 min at room temperature to afford the corresponding 2-(7-chloroquinolin-4-yl) thiosemicarbazide (3) as Click reaction as displayed in Fig. 2. The obtained compound was investigated via spectral data as; the spectrum of IR of the was displayed vibrational bands at amino and NH group at $\nu = 3390\text{ cm}^{-1}$, $\nu = 3150\text{ cm}^{-1}$; respectively, while the NH bending vibration was showed at $\nu = 1585\text{ cm}^{-1}$. Furthermore, the $^1\text{HNMR}$ of the investigated novel thiosemicarbazide was showed signals at $\delta 8.89$ due to N = CH, quinolone and singlet signal of NH_2 at $\delta 8.20$. The mass spectrum showed a peak at m/z 252 corresponding to its molecular ion (Aboelnaga and EL-Sayed, 2018).

The reactivity of 2-(7-chloroquinolin-4-yl)thiosemicarbazide (3) with ethylacetoacetate utilizing ultrasonic irradiation for 40 min at 90°C to afford the corresponding 3-(7-chloroquinolin-4-ylamino)-tetrahydro-6-methyl-2-thioxopyrimidin-4(1H)-one (4). The spectral data confirmed the obtained compound where its FT-IR spectroscopy showed stretching NH at ν

3110 cm^{-1} and bending vibration at 1587 cm^{-1} , also the C = O band showed at 1674 cm^{-1} while the C = S appeared at 1211 cm^{-1} . The $^1\text{HNMR}$ was assigned the doublet signals of N = CH quinolone at $\delta 8.20$ ppm and aromatic regions ranges between $\delta 7.15$ - 7.85 ppm. The mass spectrum of the revealed compound showed $m/z = 318$ (Aboelnaga and EL-Sayed, 2018).

Computational Studies

Molecular Orbital Calculations

The π -effects properties have an important contribution to biological systems that binding to the active site of a protein receptor so the most active optimized molecular structures of 2-(7-Chloroquinolin-4-yl)thiosemicarbazide (3) (CQT) and 3-(7-chloroquinolin-4-ylamino)-tetrahydro-6-methyl-2-thioxopyrimidin-4(1H)-one (4) (CQP) is demonstrated in Fig. 3 and selected bond lengths, bond angles and dihedral angles are scheduled in Table 3 calculated through B3LYP/6-311G (d) The molecular structure of these compound were not planar (Akl *et al.*, 2020; Fahim and Ismael, 2019; Trott and Olson, 2010). The optimized structures of CQT (3), x ray of 4,7-dichloroquinoline (Hema *et al.*, 2015) and CQP (4) as showed in Table 1 and Fig. 3.

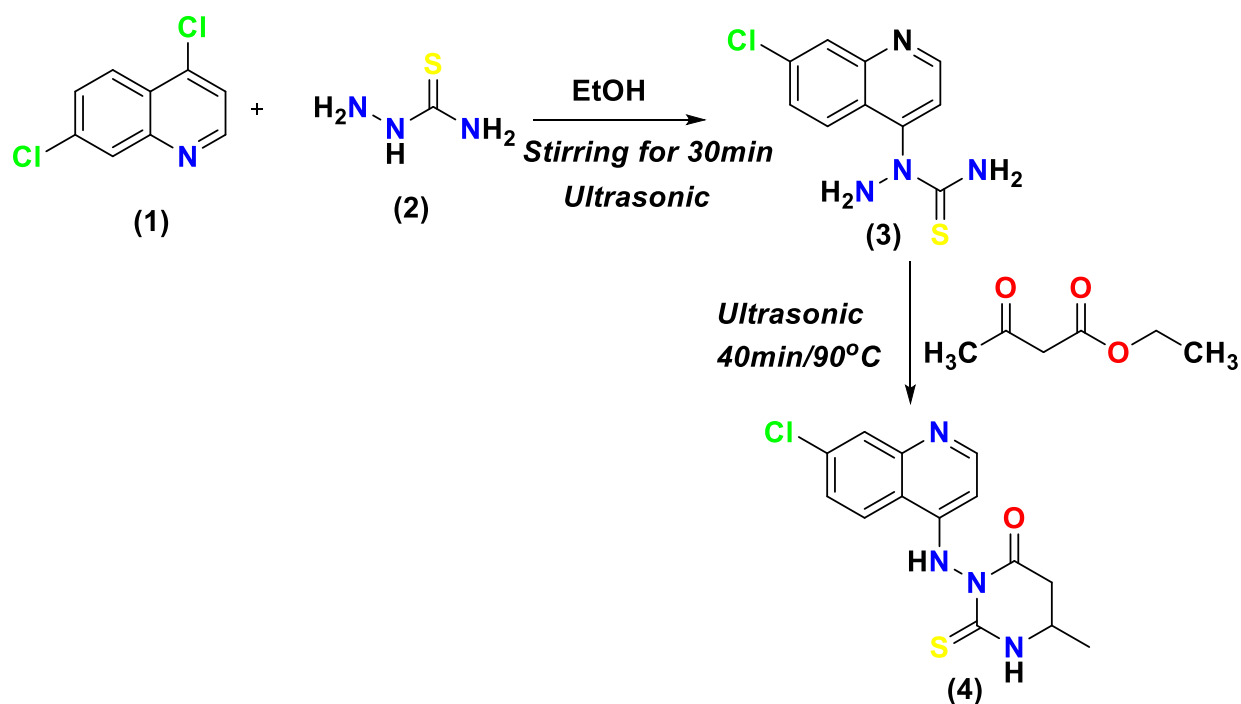


Fig. 2: (a) Ultrasonic reaction of 4,7-dichloroquinoline (1) with thiosemicarbazide (2); (b) Reactivity of 2-(7-chloroquinolin-4-yl) thiosemicarbazide (3) with ethylacetoacetate

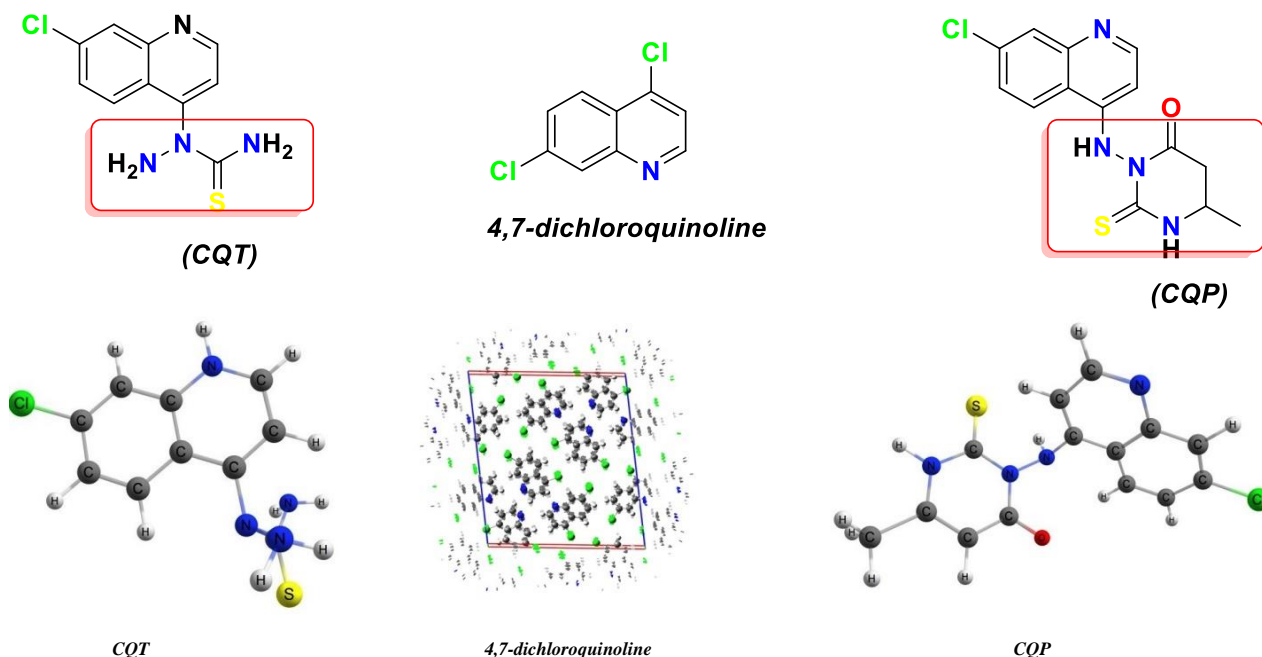


Fig. 3: The optimized geometry, numbering system and moiety of Compounds CQT (3), X ray of 4,7-dichloroquinoline (Fahim and Shalaby, 2019) and CQP(4), utilizing of DFT/B3LYP/6-311(G)-d

The optimized structure of compound CQT (3) have a different bond lengths, bond angles and dihedral angles utilizing B3LYP/6-311G(d), HF/6-311G(d). Comparing the theoretical data with the crystallographic data 4,7-dichloroquinoline (Hema *et al.*, 2015) indicated slightly alteration in the optimized bond lengths and bond angles. It was noticed that N₁₆-C₁₁ of CQT (3) measured 1.37286Å, 1.30236Å of HF/6-311G(d), B3LYP/6-311G(d); respectively while the x-ray of N_{1A}-C_{9A} (1.379 (10)Å) which the bond length of the quinolone was compatible with HF theory, but the other bonds such as C₅-C₆ (1.7600Å), (1.4023Å) for HF/6-311G(d), B3LYP/6-311G(d); respectively where it is compatible with C_{2A}-C_{3A} (1.432 (12)Å). Furthermore, the bond angles of CQT (3) such as N₁₆-C₁₁-C₁₂ (120.8622°), (120.5236°) for HF/6-311G(d), B3LYP/6-311G(d) while the x ray bond of C_{6A}-C_{5A}-C_{10A} (120.2 (8)°) which is more nearest to B3LYP/6-311G(d), also Cl₁₇-C₆-C₅ (120.64566°), (122.0236°) and the C_{3A}-C_{4A}-Cl_{1A} (119.5 (7)°). Moreover, the dihedral angles of attached thiosemicarbazide H₂₀-N₁₉-N₁₈-C₂₂ (-109.7568°), (-108.235°) and N₁₉-N₁₈-C₂₂-S₂₃(126.7877°), (128.2365°) for HF and DFT/B3LYP basis set which meant that this group out of plane and more reactive but the dihedral angle N₁₆-C₄-C₃-C₉ (-0.00075°), (-0.00072°) which compatible with the x-ray C_{9A}-N_{1A}-C_{2A}-C_{3A} (0.9(12)°) as shown in Table 1.

Also the optimized of CQP (4) and illustrated the bond lengths, angles and dihedral angles as displayed in

Table 1 and Fig. 3. The bond lengths of tetrahydro-6-methyl-2-thioxopyrimidin-4(1H)-one were utilizing B3LYP/6-311G (d), HF/6-311G (d) theory level. The bond length of N₁₇-N₂₅ (1.4700Å) (1.5912Å), (C₁₉-S₂₃) (1.56640Å) (1.3526Å) for HF and B3LYP/6-311G(d), respectively which they were mostly same included that the more delocalization of charges on tetrahydro-6-methyl-2-thioxopyrimidin-4(1H)-one with fixed bond length, while the smallest difference in bond length between theoretical and experimental of chloroquinone ring such as for C₂₂-C₂₁ for theoretical and for C_{5B}-C_{6B} of experimental was (0.0135Å) for DFT method. Also the largest difference between experimental and calculated DFT bond angles is C₅-C₆-Cl₁₆ and C_{3B}-C_{4B}-Cl_{1B} (1.3764°). Therefore, the difference of bond angles of (S₂₆-C₁₉-N₂₇), (C₁₉-N₂₇-H₂₃) between HF and DFT/B3LYP is (1.22508°), (3.24341°). Additionally, the dihedral angles of tetrahydro-6-methyl-2-thioxopyrimidin-4(1H)-one (N₂₇-C₂₂-C₂₈-H₂₉), (N₁₇-N₂₅-C₁₉-N₂₇) was taken a negative charges which were out of plane of chloroquinone and give stability of this moiety, also the dihedral of chloroquinone were compatible the theoretical and experimental (C₆-C₅-C₄-N₁₅)(-179.0236°), (C_{7B}-C_{8B}-C_{9B}-N_{1B}) (-178.5 (7)°) as displayed in Table 1. From the previous results it was noticed that the B3LYP/6-311G (d) more compatible with the confirmed structure and there are lowest difference between them (Frag and Fahim, 2019; Fahim and Shalaby, 2019; Dacrory and Fahim, 2020).

structure of these compounds was not planar. The potential activities presented in the precursor compounds CQP (4) due to presence of tetrahydro-6-methyl-2-thioxopyrimidin-4(1*H*)-one which increased the activity and more stability rather than CQT (3) due to resonance of electrons and stability of ring attached to chloroquinone. Another point of view, The π -isoelectronic structures of compound CQT (3) and CQP (4) utilizing DFT/B3LYP/6-311G(d) and HF/6-311G(d) basis set, whereas the difference in CQT between two basis set (160 eV) (≈ 3800 kcal/mol), but the CQP (4) difference was (182.126 eV) (≈ 4199.92 kcal/mol) which these difference indicate the stability of CQP (4). Moreover, the dipole moment (μ) difference for HF and B3LYP/6-311G(d) basis sets for CQT (3) through (2.9217D) and CQP (4) was (1.3353D) which indicate that the easily charge separation of CQP(4) (Atkins and De Paula, 2011) as shown in Table 2:

$$\Delta E = E_{LUMO} - E_{HOMO} \quad (1)$$

$$\chi = \frac{-(E_{LUMO} + E_{HOMO})}{2} \quad (2)$$

$$\eta = \frac{(E_{LUMO} - E_{HOMO})}{2} \quad (3)$$

$$\sigma = 1 / \eta \quad (4)$$

$$Pi = -\chi \quad (5)$$

$$S = 1 / 2\eta \quad (6)$$

$$\omega = Pi^2 / 2\eta \quad (7)$$

$$\Delta N_{max} = -Pi / \eta \quad (8)$$

The absolute electronegativities (χ) which concept that designates the affinity of an atom to attract a mutual pair of electrons, the value of (χ) for CQT (3) was (5.798 eV) (≈ 133.71286 kcal/mol) and CQP (4) was (1.1574351 eV) (≈ 26.69107 kcal/mol), which confirm that the higher value of thiosemicarbazide CQT (3) which attract the atoms of ethylacetoacetate to form the tetrahydro-6-methyl-2-thioxopyrimidin-4(1*H*)-one (Yamamoto *et al.*, 1998).

The absolute hardness (η) which measure of the resistance to change in electron density around the molecule, CQT (3) difference between HF/6-311G(d) and DFT/B3LYP/6-31G(d) (2.1739519 eV) (≈ 50.13251 kcal/mol), also the CQP (4) different (3.1191 eV) (≈ 71.9258 kcal/mol) which the more electron density of CQP and stability of this compound (Yang and Parr, 1985).

Absolute softness (σ) indicate the interaction of the compound, the difference of CQT (3) (740.1817 eV) while CQP (4) was (244.0135 eV), the large difference for CQT indicate that the activity of CQT to react with ethylacetoacetate (Fahim *et al.*, 2020).

Table 2: Ground state energies of compounds CQT (3) and CQP (4) utilizing DFT/B3LYP/6-311G(d) and HF/6-31G(d) and their physical parameters

DFT/B3LYP/6-311G(d)				HF/6-311G(d)				
Compound CQT		Compound CQP		Compound CQT		Compound CQP		
E_T (au)	-1464.3216		-1692.634	E_T (au)	-1458.83632		-1685.9406	
E_{HOMO} (au)	-0.16212		-0.24111	E_{HOMO} (au)	-0.45510		-0.31274	
E_{LUMO} (au)	-0.10736		-0.10238	E_{LUMO} (au)	-0.24055		0.05432	
E_g (eV)	1.4900962		3.7750374	E_g (eV)	5.8382057		18.24796	
μ (D)	4.6871		8.9694	μ (D)	7.6088		10.3047	
χ (eV)	3.6664639		4.67342172	χ (eV)	9.46480486		3.5159849	
η (eV)	0.7450481		1.88751869	η (eV)	2.91910283		4.9941081	
σ (eV)	993.8419		392.2795	σ (eV)	253.6602097		148.26675	
P_i (eV)	-3.6664639		-4.67342172	P_i (eV)	-9.464804857		-3.5159849	
S (eV)	0.37252405		0.94369132	S (eV)	1.459551414		2.49705403	
ω (eV)	0.06763121107		0.027837261177	ω (eV)	0.0176574768		0.04168867961	
ΔN_{max}	133.9102932		67.3727	ΔN_{max}	88.22752		19.157369	
Net charges				Net charges				
	N ₁₈	-0.384	N ₁₇	-0.465	N ₁₈	-0.510	N ₁₇	-0.544
	N ₁₉	-0.550	H ₁₈	0.352	N ₁₉	-0.605	H ₁₈	0.380
	H ₂₁	0.295	N ₂₅	-0.497	H ₂₁	0.335	N ₂₅	-0.680
	C ₂₂	-0.119	C ₁₉	0.124	C ₂₂	-0.004	C ₁₉	0.320
	H ₂₀	0.330	S ₂₆	-0.018	H ₂₀	0.377	S ₂₆	-0.084
	S ₂₃	0.056	N ₂₇	-0.681	S ₂₃	0.186	N ₂₇	-0.890
	N ₂₄	-0.679	H ₂₃	0.398	N ₂₄	-0.812	H ₂₃	0.449
			C ₂₂	0.390			C ₂₂	0.509

^a $E_g = E_{LUMO} - E_{HOMO}$.

Table 3: The calculated Mullikan and NBO charges of CQT (3) and CQP (4) utilizing DFT/ B3LYP/6-311G(d)

DFT/ B3LYP/6-311G(d)			
<i>Total Mullikan charges</i>		<i>NBO Charges</i>	
Compound CQT	Compound CQP	Compound CQT	Compound CQP
C ₁	-0.073	C ₁	0.079
C ₂	-0.062	C ₂	-0.005
C ₃	-0.191	C ₃	-0.072
C ₄	-0.434	C ₄	0.116
C ₅	-0.071	C ₅	-0.011
C ₆	-0.308	C ₆	-0.294
H ₇	0.171	Cl ₁₆	0.003
H ₈	0.176	H ₁₀	0.189
Cl ₁₇	-0.015	H ₇	0.181
H ₁₀	0.173	H ₈	0.195
N ₁₆	-0.830	N ₁₅	-0.422
H ₁₃	0.341	C ₁₁	0.039
C ₁₁	-0.124	C ₁₂	-0.168
H ₁₄	0.176	C ₉	0.209
C ₁₁	0.124	H ₁₃	0.176
C ₁₂	-0.129	H ₁₄	0.185
H ₁₅	0.131	C ₁₂	0.168
C ₉	0.342	N ₁₇	-0.465
N ₁₈	-0.384	H ₁₈	0.352
N ₁₉	-0.550	N ₂₅	-0.497
H ₂₁	0.295	C ₁₉	0.124
C ₂₂	-0.119	S ₂₆	-0.018
H ₂₀	0.330	N ₂₇	-0.681
S ₂₃	0.056	H ₂₃	0.398
N ₂₄	-0.679	C ₂₂	0.390
H ₂₅	0.325	C ₂₁	-0.298
H ₂₆	0.336	C ₂₀	0.577
		O ₃₂	-0.396
		H ₂₄	0.204
		H ₂₉	0.217
		H ₃₁	0.2220
		C ₂₈	0.610
		C ₂₂	0.390
		C ₁	-0.221
		C ₂	-0.146
		C ₃	-0.094
		C ₄	0.177
		C ₅	-0.278
		C ₆	-0.018
		Cl ₁₆	-0.002
		H ₁₀	0.240
		H ₇	0.225
		H ₈	0.195
		N ₁₅	-0.438
		C ₁₁	0.053
		C ₁₂	-0.267
		C ₉	0.184
		H ₁₃	0.201
		H ₁₄	0.226
		C ₁₂	-0.267
		N ₁₇	-0.457
		H ₁₈	0.388
		N ₂₅	-0.457
		C ₁₉	-0.270
		S ₂₆	0.212
		N ₂₇	-0.137
		H ₂₃	-0.590
		C ₂₂	0.270
		C ₂₁	0.335
		C ₂₀	0.578
		O ₃₂	-0.577
		H ₂₄	0.249
		H ₂₉	0.216
		H ₃₁	0.224
		C ₂₈	-0.596
		C ₂₂	0.772

Mullikan and NBO Atomic Charges

Mullikan and NBO of compounds CQT (3) and CQP (4) were calculated utilizing the DFT/B3LYP/6-311G(d) basis set as displayed in Table 5. For the compound the Mullikan charges of CQT(3) showed that N₁₆(-0.830) and N₂₄(-0.679) of more negative charges, while the C₉(0.342), also the NBO charges of the same compound seemed at N₁₆(-0.566), N₂₄(-0.854) and C₉(0.148) which indicated that the N₁₆ and N₂₄ are the most electrophilic centers of the thiosemicarbazide attached to chloroquinoline moiety and the attached Carbon C₉ of chloroquinone which act as nucleophilic susceptibility center which make stability of quinolone ring as displayed in Table 3. Furthermore, the Mullikan and NBO charges of CQP (4) compound showed the most electrophilic negative center of moiety of tetrahydro-6-methyl-2-thioxopyrimidin-4(1*H*)-one moiety which attached to quinolone ring which showed the N₁₇(-0.465),

N₂₅(-0.497), S₂₆(-0.018) and N₂₇(-0.681) for Mullikan while N₁₇(-0.457), N₂₅(-0.457), S₂₆(0.212) and N₂₇(-0.137) which meant that the stability of thiopyrimidine moiety with quinolone ring (Ibrahim and Mahmoud, 2009).

Frontier Molecular Orbitals (FMO) and Molecular Electrostatic Potential Maps (ESP)

The electrical and optical properties can be inferred through chemical reactions and ultraviolet spectra, but FMO is an amazing guideline method for identifying these properties. Time-Dependent Functional Density Theory (TD-DFT) is used for studying FMO principles (Griffith and Orgel, 1957) The highest occupied HOMO molecular orbital acts as an electron donor and the LUMO lowest unoccupied molecular orbital acts as an electron acceptor مرجع. The energy difference between HOMOs and LUMOs related to the biological activity of the molecule (Dennington *et al.*, 2009). Additionally, it

helps in describing the molecule reactivity and kinetic stability. The high kinetic stability is due to the large energy gap between HOMO-LUMO (Gaussian09, 2009). Figure 6 illustrates the distributions and energy levels of the HOMO, LUMO and orbitals computed at the B3LYP/6-311G (d) level for CQT and CQP. The positive and negative phases were symbolized in red and green colors, respectively. As shown in Fig. 4, the HOMO of compound CQT was localized in the fused of quinolone ring and its LUMO was localized in the N-atom of quinolone moiety, the value of the energy gap between the HOMO -LUMO is (1.49 eV). Furthermore, the HOMO and LUMO of CQP was localized on Sulphur atom of tetrahydro-6-methyl-2-thioxopyrimidin-4(1H)-one ring with difference in band energy (3.77 eV). This energy gap between HOMO-LUMO indicates the high excitation energies for a lot of excited states and reactivity of these compounds. Moreover, molecular reactivity and biological recognition interactions can be studied by the molecular Electrostatic Potential (ESP) that the nuclei and electrons of a molecule create in the surrounding space (Fukui, 1982). So, the 3-(7-chloroquinolin-4-ylamino)-tetrahydro-6-methyl-2-thioxopyrimidin-4(1H)-one (4) (CQP) designate a certain point then gather this to remaining surface, indicates that there is a uniform distribution of surface

contour to fused quinolone, whereas the methyl-2-thioxopyrimidin-4(1H)-one moiety contains the C = O and C = S which acts as electrophilic centers which induced more protonation and gave more reactivity in the biological interaction and in the binding sites of proteins in molecular docking (Schlegel, 1982) as demonstrated in Fig. 4.

Biological Investigation

Antimalarial Activity

The investigated compounds CQT (3) and CQP (4) were previously treated against action of *P. falciparum* as displayed in Table 4. The CQT and CQP showed higher antimalarial activity in yield for CQT with (80% yield, $IC_{50} = 25.37 \mu\text{g/mL}$) and CQP (87% yield, $IC_{50} = 11.92 \mu\text{g/mL}$) as shown in Table 4 and Fig. 5. The preliminary SAR study of CQP has focused on the influence of occurrence methyl-2-thioxopyrimidin-4(1H)-one moiety attached to chloroquinoline and make more polarizable of electrons and enhancing their antimalarial activities, while the CQT with low activity due to presence of NH_2 attached of C = S of thiosemicarbazide and more electrons center which increase the activity (Bawa *et al.*, 2010).

Table 4: The invitro- antimalrial activity of CQT and CQP against plasmodium falciparum

Compound	Yield (%)	IC_{50}
CQT	80	25.37
CQP	87	11.92
CQ	100	0.18

CQ: Chloquinone drug

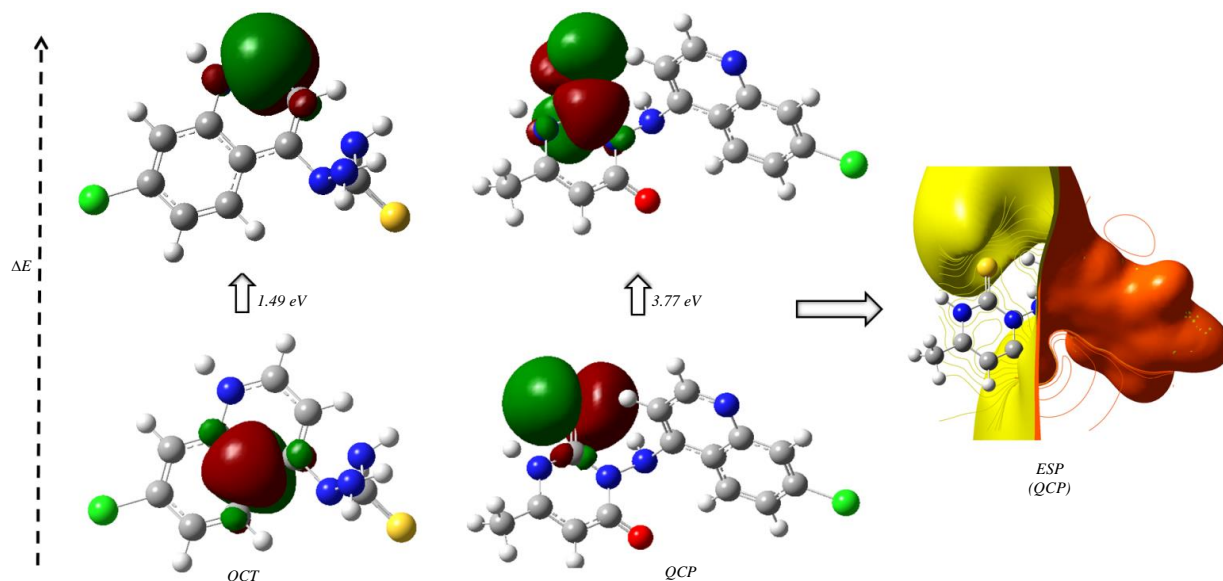


Fig. 4: FMO and ESP of CQT and CQP at (TD-DFT) B3LYP/ 6-311G (d) basis sets

Molecular Docking Studies

A molecular modeling study was carried out to explain the cytotoxic activity profile demonstrated by the synthesized compounds. A conformational search using an implicit solvent model was accomplished for the prepared compounds; this was monitored by the refinement of the geometry of local minima through a Quantum-Mechanical (QM) (Morris *et al.*, 2009). Consequently, adaptable docking of the compounds was cultivated in the crystal structure of the (PDBID: 6LU7 Version 2, 2.16 Å resolution, CQP (4) was stimulated with functions as a homo dimer (Jin *et al.*, 2020) and leads that target main protease (Mpro) of SARS-CoV-2: Mpro is a key enzyme of coronaviruses and has a pivotal role in mediating viral replication and transcription, making it an attractive drug target for SARS-CoV-25,6 (Jo *et al.*, 2020). The docking simulation of CQT and CQP with (PDBID: 6lu7) as shown in Table 5 and Fig. 6 to evaluate the binding interaction energy and the distance between protein's and it was shown that the (PDBID: 6lu7) attached to CQP with ($\Delta E = -14.4383$ Kcal/mol, 2.337Å) with Hydrogen bonding with amino acid Pro132 of NH

group rather than the CQT attached with binding energy ($\Delta E = -12.2755$ Kcal/mol, 3.576Å) and attached to chloroquinoline with Phe294. We identified a mechanism-based inhibitor (N3) through docking stimulation and determined that the crystal structure of Mpro of SARS-CoV-2 in complex with CQT and CQP. Through a combination of structure-based virtual and high-throughput screening, Furthermore, crystal structure of a protein of unknown function TA1206 from thermoplasma acidophilum (PDBID: 1qw2O) (Pathare *et al.*, 2017) which contain of single unique chain 1qw2(A) (102 residues long) (Pathare *et al.*, 2017). The compounds CQT and CQP were docked with (PDBID: 1qw2) with binding interaction energy ($\Delta E = -6.66, -13.61$ kcal/mol); respectively and with short bond distance of CQP with 2.51Å with NH between chloroquinone and tetrahydro-6-methyl-2-thioxopyrimidin-4(1H)-one ring which confirmed this H-proton the most active in mobilization of electrons and increase the biological evaluation of Compound CQP rather than CQT which its docking ability with (PDBID: 1qw2) with NH₂ groups and bond distance 3.21Å as shown in Table 5 and Fig. 6.

Table 5: Docking of CQT(3) and CQP(4) with (PDB ID: 6lu7) and (PDBID:1q2w):

Compound	Energy affinity (kcal/mol)	Distance (Å)	Amino acids
PDBID: 6lu7			
CQT	-12.2755	3.576	Gln110,Ph294,Asn 151, Ser158, Asp153 and Asn 133
CQP	-14.4383	2.337	Pro132, Thr196, Asp153, Asn 133, Glu240 and Thr 198
PDBID: 1q2w(Chain A)			
CQT	-6.6601	3.21	Pro108, His 246, GlnA107
CQP	-13.6197	2.51	Pro A108, GluA240,HisA246 and Leu202

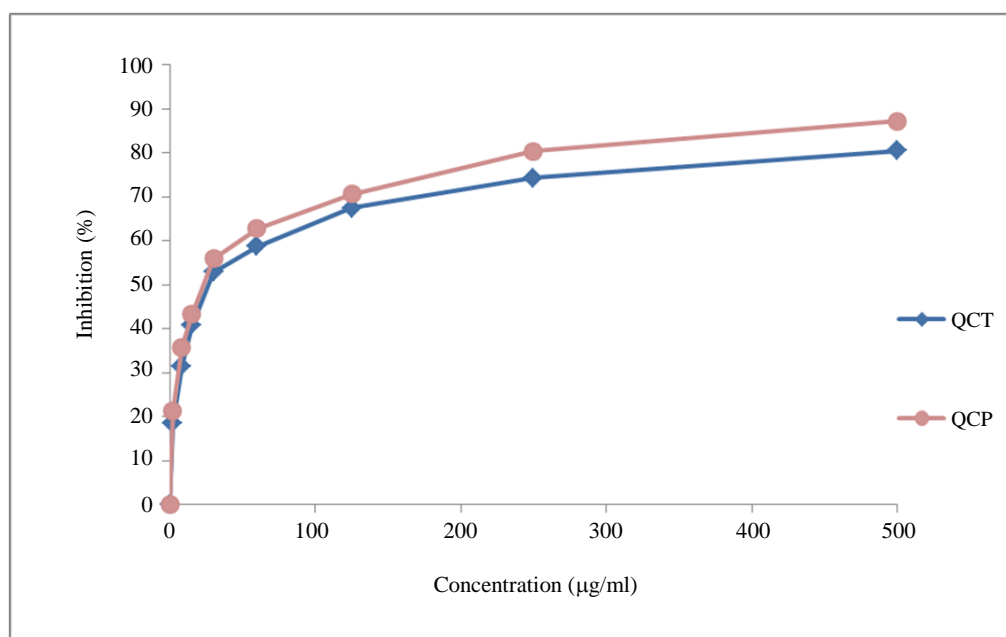


Fig. 5: The antimalarial concentration of CQT (3) and CQP (4)

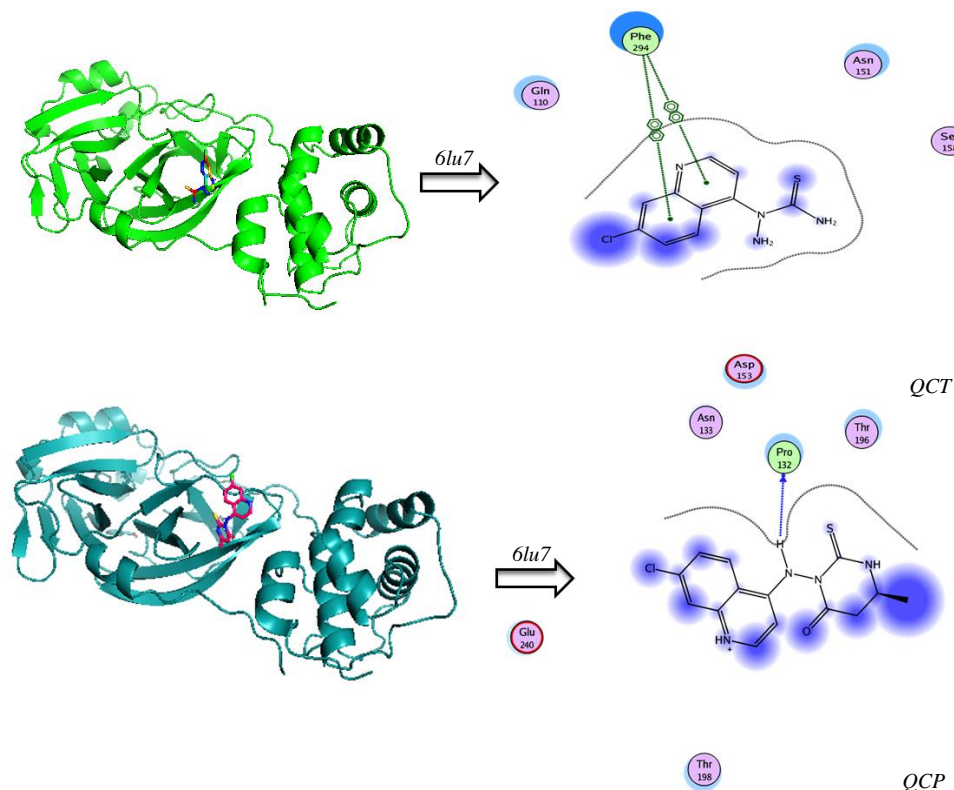


Fig. 6: Binding docking modes of CQT, CQP with (a) PDBID: 6lu7 and (b) PDBID:1qw2; respectively

Experimental

General Procedure

Melting points were measured with a Gallen Kamp melting point apparatus. Silica-gel-coated aluminum plates used to test the purity of the compounds. Infrared spectra ($\lambda\text{-cm}^{-1}$) were recorded on Bruker Vector (Germany) and on Mattson FT-IR 1000 (Cairo University, Egypt), using KBr disks. ^1H NMR spectra were recorded on Gemini 300 MHz, ^{13}C NMR spectrometer, in DMSO-d_6 using dimethyl sulfoxide as a solvent and tetramethylsilane (TMS) as an internal standard (Chemical shift in δ , ppm); ^{13}C NMR spectra were recorded on Gemini 50 MHz NMR spectrometer. Mass spectra were measured on GCQ Finnigan MAT and Elemental analyses were performed at the micro analytical Center, Cairo University, Giza, Egypt. Biological activity was determined in a laboratory by the Regional Center for Mycology and Biotechnology (RCMB), Al-Azhar University, Cairo, Egypt. All the chemicals were purchased from Sigma-Aldrich.

Synthesis of 2-(7-Chloroquinolin-4-yl)Thiosemicarbazide (3)

An ethanolic solution of 4,7-dichloroquinoline (1) (0.196 g, 0.01 mol) with thiosemicarbazide (2) (0.096,

0.01 mole) were stirred in ultrasonic apertures at room temperature for 30 min, then monitoring TLC to know the reaction was finished then add CH_3Cl and washed with solution NaOH solution to afford the organic layer and aqueous layer. Then the crude poured on ice bath to afford 2-(7-chloroquinolin-4-yl)thiosemicarbazide (3): yellow soild which was washed with ether and dried. Yield: 80%; mp 278-280°C, $R_f = 0.38$ (1:2 EtOAc-petroleum ether); IR (KBr) cm^{-1} : 3390-3266 (NH_2), 3150 (NH), 1615 ($\text{C} = \text{N}$), 1585 (NH_{bend}), 1235 ($\text{C}-\text{N}$), 1212 ($\text{C} = \text{S}$), 758 ($\text{C}-\text{Cl}$); ^1H NMR(300 MHz, DMSO-d_6) δ 8.89(d, $J = 5.48$ Hz, 1H, N = CH, quinoline), 8.57(d, $J = 8.48$ Hz, 1H, Ar-H), 8.54(s, 1H, Ar-H), 8.26(d, $J = 8.43$ Hz, 1H, Ar- H), 8.20 (s, 2H, NH_2), 8.10 (s, 1H, ArC-NH), 7.93(d, $J = 5.42$ Hz, 1H, Ar-H), 7.86 (s, 1H, NH); ^{13}C NMR(50 MHz, DMSO-d_6) 181.22, 158.22, 155.72, 149.02, 148.14, 138.50, 128.42, 127.65, 120.03, 18.34. Mass spectra (M^+) $m/z = 252$. Anal. Calcd for $\text{C}_{10}\text{H}_9\text{ClN}_4\text{S}$: C, 47.53; H, 3.59; N, 22.17. Found: C, 47.33; H, 3.52; N, 22.09%.

Reactivity of 2-(7-Chloroquinolin-4-yl)Thiosemicarbazide (3) with Ethyl Acetoacetate

Ultrasonic reaction of compound (3) (0.25 g, 0.01 mol) with ethylacetoacetate (2 mL, 0.01 mol) in water bath for 40 min at 90°C, the solid product was formed

and filtered to afford the corresponding product (4) and crystallized with EtOH 3-(7-chloroquinolin-4-ylamino)-tetrahydro-6-methyl-2-thioxopyrimidin-4(1H)-one (4): Brown crystals which was washed with ether and dried. Yield: 87%; mp 250-252°C Rf = 0.48(1:2 EtOAc-petroleum ether); IR (KBr) cm^{-1} : 3110 (NH), 1674 (C = O), 1618 (C = N), 1587 (NH bend), 1237 (C-N), 1211 (C = S), 760(C-Cl) ; ^1H NMR(300 MHz, DMSO- d_6): δ 8.20 (d, J = 5.38 Hz, ^1HN = CH quinoline) 8.10 (s, ^1H , NH), 7.85 (d, J = 8.32 Hz, ^1H , Ar- H), 7.82 (s, ^1H , Ar- H), 7.18 (d, J = 5.38 Hz, ^1H , Ar- H), 7.15 (d, J = 5.38 Hz, ^1H , Ar- H), 2.50 (s, 2H, CH_2), 2.17 (s, 3H, CH_3); ^{13}C NMR (50 MHz, DMSO- d_6) δ 181.36, 166.23, 156.96, 151.13, 149.15, 141.30, 138.57, 122.23, 119.52, 118.17, 115.31, 113.80, 91.21, 48.79. Mass spectra (M^+) m/z = 318. Anal. Calcd. for $\text{C}_{14}\text{H}_{11}\text{N}_4\text{ClO}_2$: C, 52.75; H, 3.48; N, 17.58. Found: C, 52.91; H, 3.32; N, 17.71%.

Determination of Antimalarial Activity

Cultures of *P. falciparum* were measured according to a protocol from (Moloney *et al.*, 1990; Trager and Williams, 1992). The percentage of Inhibition was studied the 50% inhibitory concentrations (IC_{50}) was measured and the data got from the inhibitor-dependent concentration growth curves were registered into plots with nonlinear retreating analysis from y-axis (inhibition %) to x-axis (inhibitor concentration) (Singh *et al.*, 1997) *P. falciparum* isolate NF54 was maintained in continuous culture with gentamicin (40 $\mu\text{g}/\text{mL}$) in Petri dishes (5 cm in diameter) with a gaseous phase of 90% N_2 , 5% O_2 and 5% CO_2 , according to a protocol from (Moloney *et al.*, 1990; Trager and Williams, 1992) *P. falciparum* parasites were cultured in human erythrocytes (blood group A+ at 10% (v/v) hematocrit) in RPMI 1640 medium (Sigma) supplemented with 25 mM HEPES, 20 mM sodium bicarbonate and 10% heat-inactivated human A+ plasma. The culture was routinely monitored through Giemsa staining of the thin blood smears. The parasitemia of the infected erythrocytes was determined in Giemsa-stained smears by light microscopy. Parasitemias and morphological changes detected in the cultures were scored visually with a 100-fold oil-immersion objective, counting at least 1000 erythrocytes to determine the percentage of the infected erythrocytes (Kaiser *et al.*, 2003). Antimalarial activity assay: The experiments were performed in 96-well culture plates (Nunc); compounds were tested at two-fold dilutions in a dose-titration range of 500 to 2 μM . One hundred microliters of infected human red blood cell suspension (1% parasitemia, 4% hematocrit), with more than 90% of ring forms, were added to each well containing 100 μL of extracts pre-diluted in RPMI-1640. Test plates were incubated for 48 h. Parasite multiplication was determined microscopically after Giemsa staining and

expressed as a percentage of the controls without test compounds. A drug-free control (methanol/water 50:50% v,v) was used in all experiments and CQ (0.01 μM) was used as the standard reference drug. Parasitemia and stage distribution were estimated as triplicates daily from Giemsa-stained smears by counting 1000 erythrocytes (Noedl *et al.*, 2002).

Computational Procedures

Calculations of DFT with a hybrid functional B3LYP (Becke's three-parameter hybrid functional using the BLYP correlation functional) with the 6-311G(d) basis set and Hartree-Fock calculations with the 6-311G(d) basis set using the Berny method (Jamróz, 2013), were performed with the Gaussian 09 W program (Ditchfield, 1972). No symmetry constraints were applied during the geometry optimization. The harmonic vibrational frequencies were calculated at the same level of theory for the optimized structures to prove the optimized structures as true minimums and confirm that no imaginary frequency occurs. The wideranging assignments of the vibrational modes were accomplished on the basis of the Potential Energy Distribution (PED), calculated using Vibrational Energy Distribution Analysis (VEDA) program (Foresman and Frish, 1996).

Molecular Docking

The molecular model of innovative sulfonamide derivatives was fabricated using standard bond lengths and angles, with the AutoDock Vina and detected by Discovery Studio Client (version 4.2). Following geometry optimization, a systematic conformational examine was supported out to an RMS gradient of 0.01 \AA , with energy minimization of the resultant conformations employing the Confirmation Examination module implemented in Auto Dock Vina. The experimental Structure of Mpro from SARS-CoV-2 and discovery of its inhibitors (PDBID: 6lu7) (Jo *et al.*, 2020) and Crystal structure of a protein of unknown function ta1206 from thermoplasma acidophilum (PDBID: 1qw2) (Pathare *et al.*, 2017). Missing hydrogens were added to the enzyme and partial charges were considered. After removing the co-crystallized inhibitor, validation monitored by docking of the compounds were carried out by AutoDock Vina and viewed by Discovery Studio Client (version 4.2) (Morris *et al.*, 2009). The goal protein was kept inflexible, while the ligands were disappeared permitted to determine the conformational space exclusive the enzyme cavity; Twenty dispersed docking simulations were run via default parameters and the confirmations were designated constructed on the arrangement of total statistics, E conformation and appropriate with the relevant amino acids in the binding pocket.

Conclusion

In this study, the synthesis of some novel chloroquinoline derivative using green methodology, the synthesized compounds were exhibited high antimalarial activities. The SAR relationship related to the most active compound was CQP (4) with $IC_{50} = 11.92 \mu\text{g/ml}$ and due to cyclized tetrahydro-6-methyl-2-thioxopyrimidin-4(1*H*)-one ring attached to chlorine ring. The optimized molecular structure of compounds CQT and CQP utilizing of DFT/B3LYP/6-311G(d) and HF/6-311G(d) basis's set, approves their stability and the geometric parameters suggestions between the calculated and the experimental data values indicate that B3LYP basis set is better than the HF method in approximating bond lengths and in evaluating energy, Mullikan and NBO charges. Furthermore, the CQT and CQP were docked against (PDB ID: 6lu7) and (PDBID: 1q2w) and showed the NH-hydrogen: 2.337\AA of CQP with (Mpro) of SARS-CoV-2. So for further biological investigation we will test these compounds and other quinolone derivatives in treatment of SARS-Covid-19.

Acknowledgment

The authors thanks Departement of chemistry Faculty of Women of Arts, Science and Education, Ain Shams University and Departments of Green Chemistry, National Research Center for scientific contribution

Author's Contributions

Asmaa Aboelnaga: Preparation of organic compounds and main corresponding author.

Asmaa M. Fahim: Make theoretical studies and elucidation the main idea of manuscript.

Taghreed H. EL-Sayed: Synthesis the organic compounds and revise the manuscript.

Ethics

This article is original and contains unpublished material. The corresponding author confirms that all of the other authors have read and approved the manuscript and no ethical issues involved.

References

Aboelnaga, A., & EL-Sayed, T. H. (2018). Click synthesis of new 7-chloroquinoline derivatives by using ultrasound irradiation and evaluation of their biological activity. *Green Chemistry Letters and Reviews*, 11(3), 254-263.

Adem, S., Eyupoglu, V., Sarfraz, I., Rasul, A., & Ali, M. (2020). Identification of potent COVID-19 main protease (Mpro) inhibitors from natural polyphenols: An in silico strategy unveils a hope against CORONA.

Akl, E. M., Dacrory, S., Abdel-Aziz, M. S., Kamel, S., & Fahim, A. M. (2020). Preparation and characterization of novel antibacterial blended films based on modified carboxymethyl cellulose/phenolic compounds. *Polymer Bulletin*, 1-25.

Arif, R., Rana, M., Yasmeen, S., Khan, M. S., Abid, M., & Khan, M. S. (2020). Facile synthesis of chalcone derivatives as antibacterial agents: Synthesis, DNA binding, molecular docking, DFT and antioxidant studies. *Journal of Molecular Structure*, 1208, 127905.

Atkins, P., & De Paula, J. (2011). *Physical chemistry for the life sciences*. Oxford University Press, USA.

Bawa, S., Kumar, S., Drabu, S., & Kumar, R. (2010). Structural modifications of quinoline-based antimalarial agents: Recent developments. *Journal of Pharmacy and Bioallied Sciences*, 2(2), 64.

Bzówka, M., Mitusinska, K., Raczynska, A., Samol, A., Tuszyński, J. A., & Góra, A. (2020a). Molecular Dynamics Simulations Indicate the COVID-19 Mpro Is Not a Viable Target for Small-Molecule Inhibitors Design. *bioRxiv*.

Bzówka, M., Mitusińska, K., Raczynska, A., Samol, A., Tuszyński, J. A., & Góra, A. (2020b). Structural and Evolutionary Analysis Indicate That the SARS-CoV-2 Mpro Is a Challenging Target for Small-Molecule Inhibitor Design. *International journal of molecular sciences*, 21(9), 3099.

Chen, Y. W., Yiu, C. P. B., & Wong, K. Y. (2020). Prediction of the SARS-CoV-2 (2019-nCoV) 3C-like protease (3CL pro) structure: virtual screening reveals velpatasvir, ledipasvir and other drug repurposing candidates. *F1000Research*, 9.

Dacrory, S., & Fahim, A. M. (2020). Synthesis, anti-proliferative activity, computational studies of tetrazole cellulose utilizing different homogenous catalyst. *Carbohydrate Polymers*, 229, 115537.

Dennington, R., Keith, T., & Millam, J. G. (2009). version 5; Semichem Inc. Shawnee Mission, KS.

Ditchfield, R. (1972). Molecular orbital theory of magnetic shielding and magnetic susceptibility. *The Journal of Chemical Physics*, 56(11), 5688-5691.

dos Santos Chagas, C., Fonseca, F. L., & Bagatin, I. A. (2019). Quinoline-derivative coordination compounds as potential applications to antibacterial and antineoplastic drugs. *Materials Science and Engineering: C*, 98, 1043-1052.

Fahim, A. M., & Shalaby, M. A. (2019). Synthesis, biological evaluation, molecular docking and DFT calculations of novel benzenesulfonamide derivatives. *Journal of Molecular Structure*, 1176, 408-421.

Fahim, A. M., Wasiniak, B., & Łukaszewicz, J. P. (2020). Molecularly Imprinted Polymer and Computational Study of (E)-4-(2-cyano-3-(dimethylamino) acryloyl) benzoic Acid from Poly (ethylene terephthalate) Plastic Waste. *Current Analytical Chemistry*, 16(2), 119-137.

- Fahim, A., & Ismael, E. (2019). Synthesis, Antimicrobial Activity and Quantum Calculations of Novel Sulphonamide Derivatives. *Egyptian Journal of Chemistry*, 62(8), 1427-1440.
- Farag, A. M., & Fahim, A. M. (2019). Synthesis, biological evaluation and DFT calculation of novel pyrazole and pyrimidine derivatives. *Journal of Molecular Structure*, 1179, 304-314.
- Fehr, A. R., & Perlman, S. (2015). Coronaviruses: an overview of their replication and pathogenesis. In *Coronaviruses* (pp. 1-23). Humana Press, New York.
- Foresman, J., & Frish, E. (1996). *Exploring chemistry*. Gaussian Inc., Pittsburg, USA.
- Fukui, K. (1982). Role of frontier orbitals in chemical reactions. *science*, 218(4574), 747-754.
- Gaussian09, R. A. (2009). 1, mj frisch, gw trucks, hb schlegel, ge scuseria, ma robb, jr cheeseman, g. Scalmani, v. Barone, b. Mennucci, ga petersson *et al.*, gaussian. Inc., Wallingford CT, 121, 150-166.
- Gimeno, A., Ojeda-Montes, M. J., Tomás-Hernández, S., Cereto-Massagué, A., Beltrán-Debón, R., Mulero, M., ... & Garcia-Vallvé, S. (2019). The light and dark sides of virtual screening
- Griffith, J. S., & Orgel, L. E. (1957). Ligand-field theory. *Quarterly Reviews, Chemical Society*, 11(4), 381-393.
- Grimstein, M., Yang, Y., Zhang, X., Grillo, J., Huang, S. M., Zineh, I., & Wang, Y. (2019). Physiologically based pharmacokinetic modeling in regulatory science: an update from the US Food and Drug Administration's Office of Clinical Pharmacology. *Journal of pharmaceutical sciences*, 108(1), 21-25.
- Guo, Y. R., Cao, Q. D., Hong, Z. S., Tan, Y. Y., Chen, S. D., Jin, H. J., ... & Yan, Y. (2020). The origin, transmission and clinical therapies on coronavirus disease 2019 (COVID-19) outbreak—an update on the status. *Military Medical Research*, 7(1), 1-10.
- Hagar, M., Chaieb, K., Parveen, S., Ahmed, H. A., & Alnoman, R. B. (2020). N-alkyl 2-pyridone versus O-alkyl 2-pyridol: Ultrasonic synthesis, DFT, docking studies and their antimicrobial evaluation. *Journal of Molecular Structure*, 1199, 126926.
- Hema, R., Parthasarathi, V., Ravikumar, K., Nallu, M., & Sarkunam, K. (2015). *Acta Crystallographica Section E Structure Reports Online* ISSN 1600-5368.
- Hosseini, F. S., & Amanlou, M. (2020). Simeprevir, potential candidate to repurpose for coronavirus infection: virtual screening and molecular docking study.
- Ibrahim, M., & Mahmoud, A. A. (2009). Computational notes on the reactivity of some functional groups. *Journal of Computational and Theoretical Nanoscience*, 6(7), 1523-1526.
- Jamróz, M. H. (2013). Vibrational energy distribution analysis (VEDA): scopes and limitations. *Spectrochimica Acta Part A: Molecular and Biomolecular Spectroscopy*, 114, 220-230.
- Jin, Z., Du, X., Xu, Y., Deng, Y., Liu, M., Zhao, Y., ... & Duan, Y. (2020). Structure of Mpro from COVID-19 virus and discovery of its inhibitors. *bioRxiv*. Preprint.
- Jo, S., Kim, S., Shin, D. H., & Kim, M. S. (2020). Inhibition of SARS-CoV 3CL protease by flavonoids. *Journal of enzyme inhibition and medicinal chemistry*, 35(1), 145-151.
- Kaiser, A., Gottwald, A., Maier, W., & Seitz, H. M. (2003). Targeting enzymes involved in spermidine metabolism of parasitic protozoa—a possible new strategy for anti-parasitic treatment. *Parasitology Research*, 91(6), 508-516.
- Khaerunnisa, S., Kurniawan, H., Awaluddin, R., Suhartati, S., & Soetjipto, S. (2020). Potential inhibitor of COVID-19 main protease (Mpro) from several medicinal plant compounds by molecular docking study. *Prepr. doi10, 20944, 1-14*.
- Kong, R., Yang, G., Xue, R., Liu, M., Wang, F., Hu, J., ... & Chang, S. (2020). COVID-19 Docking Server: An interactive server for docking small molecules, peptides and antibodies against potential targets of COVID-19. *arXiv preprint arXiv:2003.00163*.
- Kwofie, S. K., Broni, E., Dankwa, B., Enniful, K. S., Teye, J., Davidson, C. R., ... & Miller, W. A. (2020). Review of Atypical Organometallic Compounds as Antimalarial Drugs. *Journal of Chemistry*, 2020.
- Liu, J., Cao, R., Xu, M., Wang, X., Zhang, H., Hu, H., ... & Wang, M. (2020). Hydroxychloroquine, a less toxic derivative of chloroquine, is effective in inhibiting SARS-CoV-2 infection in vitro. *Cell discovery*, 6(1), 1-4.
- Liu, X., & Wang, X. J. (2020). Potential inhibitors against 2019-nCoV coronavirus M protease from clinically approved medicines. *Journal of Genetics and Genomics*, 47(2), 119.
- Ludwig, S., & Zarbock, A. (2020). Coronaviruses and SARS-CoV-2: A Brief Overview. *Anesthesia and Analgesia*.
- Mirza, M. U., & Froeyen, M. (2020). Structural elucidation of SARS-CoV-2 vital proteins: Computational methods reveal potential drug candidates against main protease, Nsp12 polymerase and Nsp13 helicase. *Journal of Pharmaceutical Analysis*.
- Moloney, M. B., Pawluk, A. R., & Ackland, N. R. (1990). *Plasmodium falciparum* growth in deep culture. *Transactions of the Royal Society of Tropical Medicine and Hygiene*, 84(4), 516-518.
- Morris, G. M., Huey, R., Lindstrom, W., Sanner, M. F., Belew, R. K., Goodsell, D. S., & Olson, A. J. (2009). AutoDock4 and AutoDockTools4: Automated docking with selective receptor flexibility. *Journal of computational chemistry*, 30(16), 2785-2791.
- Noedl, H., Wernsdorfer, W. H., Miller, R. S., & Wongsrichanalai, C. (2002). Histidine-rich protein II: a novel approach to malaria drug sensitivity testing. *Antimicrobial agents and chemotherapy*, 46(6), 1658-1664.

- Pathare, G. R., Nagy, I., Hubert, A., Thomas, D. R., & Bracher, A. (2017). Crystal structure of the *Thermoplasma acidophilum* protein Ta1207. *Acta Crystallographica Section F: Structural Biology Communications*, 73(6), 328-335.
- Rodriguez-Morales, A. J., Bonilla-Aldana, D. K., Balbin-Ramon, G. J., Rabaan, A. A., Sah, R., Paniz-Mondolfi, A., ... & Esposito, S. (2020). History is repeating itself: Probable zoonotic spillover as the cause of the 2019 novel Coronavirus Epidemic. *Infez Med*, 28(1), 3-5.
- Schlegel, H. B. (1982). Optimization of equilibrium geometries and transition structures. *Journal of Computational Chemistry*, 3(2), 214-218.
- Singh, S., Puri, S. K., Singh, S. K., Srivastava, R., Gupta, R. C., & Pandey, V. C. (1997). Characterization of Simian Malarial Parasite (*Plasmodium knowlesi*)-induced Putrescine Transport in Rhesus Monkey Erythrocytes a novel putrescine conjugate arrests in vitro growth of simian malarial parasite (*plasmodium knowlesi*) and cures multidrug resistant murine malaria (*plasmodium yoelii*) infection in vivo. *Journal of Biological Chemistry*, 272(21), 13506-13511.
- Sjödín, H., Wilder-Smith, A., Osman, S., Farooq, Z., & Rocklöv, J. (2020). Only strict quarantine measures can curb the coronavirus disease (COVID-19) outbreak in Italy, 2020. *Eurosurveillance*, 25(13), 2000280.
- Steardo, L., Steardo Jr, L., Zorec, R., & Verkhatsky, A. (2020). Neuroinfection may contribute to pathophysiology and clinical manifestations of COVID-19. *Acta Physiologica*, e13473.
- Tang, B., He, F., Liu, D., Fang, M., Wu, Z., & Xu, D. (2020). AI-aided design of novel targeted covalent inhibitors against SARS-CoV-2. *bioRxiv*.
- Ton, A. T., Gentile, F., Hsing, M., Ban, F., & Cherkasov, A. (2020). Rapid identification of potential inhibitors of SARS-CoV-2 main protease by deep docking of 1.3 billion compounds. *Molecular informatics*.
- Trager, W., & Williams, J. (1992). Extracellular (axenic) development in vitro of the erythrocytic cycle of *Plasmodium falciparum*. *Proceedings of the National Academy of Sciences*, 89(12), 5351-5355.
- Trott, O., & Olson, A. J. (2010). AutoDock Vina: improving the speed and accuracy of docking with a new scoring function, efficient optimization and multithreading. *Journal of computational chemistry*, 31(2), 455-461.
- Wu, F., Zhao, S., Yu, B., Chen, Y. M., Wang, W., Song, Z. G., ... & Yuan, M. L. (2020a). A new coronavirus associated with human respiratory disease in China. *Nature*, 579(7798), 265-269.
- Wu, C., Liu, Y., Yang, Y., Zhang, P., Zhong, W., Wang, Y., ... & Zheng, M. (2020b). Analysis of therapeutic targets for SARS-CoV-2 and discovery of potential drugs by computational methods. *Acta Pharmaceutica Sinica B*.
- Xu, Z., Peng, C., Shi, Y., Zhu, Z., Mu, K., Wang, X., & Zhu, W. (2020). Nelfinavir was predicted to be a potential inhibitor of 2019-nCoV main protease by an integrative approach combining homology modelling, molecular docking and binding free energy calculation. *BioRxiv*.
- Yamamoto, K., Sawanishi, H., & Miyamoto, K. I. (1998). Structure-activity relationships of alkylxanthine inhibitors of phosphodiesterase IV isoenzyme. *Biological and Pharmaceutical Bulletin*, 21(4), 356-359.
- Yang, P., & Wang, X. (2020). COVID-19: a new challenge for human beings. *Cellular & molecular immunology*, 17(5), 555-557.
- Yang, W., & Parr, R. G. (1985). Hardness, softness and the Fukui function in the electronic theory of metals and catalysis. *Proceedings of the National Academy of Sciences*, 82(20), 6723-6726.
- Yao, X., Ye, F., Zhang, M., Cui, C., Huang, B., Niu, P., ... & Zhan, S. (2020). In vitro antiviral activity and projection of optimized dosing design of hydroxychloroquine for the treatment of severe acute respiratory syndrome coronavirus 2 (SARS-CoV-2). *Clinical Infectious Diseases*.
- Yoshino, R., Yasuo, N., & Sekijima, M. (2020). Identification of key interactions between SARS-CoV-2 Main Protease and inhibitor drug candidates.
- Zhao, S., Lin, Q., Ran, J., Musa, S. S., Yang, G., Wang, W., ... & Wang, M. H. (2020). Preliminary estimation of the basic reproduction number of novel coronavirus (2019-nCoV) in China, from 2019 to 2020: A data-driven analysis in the early phase of the outbreak. *International journal of infectious diseases*, 92, 214-217.
- Zhou, P., Yang, X. L., Wang, X. G., Hu, B., Zhang, L., Zhang, W., ... & Chen, H. D. (2020). A pneumonia outbreak associated with a new coronavirus of probable bat origin. *nature*, 579(7798), 270-273.